enhancement of the ^{176}Lu decay by gamma-induced photoexcitation (*29*). Most chondritic phosphates have ages similar to or younger than the Richardton and Acapulco phosphates analyzed here (*26*) and thus postdate the proposed photoexcitation. In this case, the slope of a whole rock chondritic Lu-Hf isochron is expected to be similar to the slopes of meteoritic phosphate isochrons.

References and Notes

1. F. Begemann *et al.*, *Geochim. Cosmochim. Acta* **65**, 111 (2001).
2. U. Söderlund, P. J. Patchett, J. D. Vervoort, C. E. Isachsen, *Earth Planet. Sci. Lett.* **219**, 311 (2004).
3. P. J. Patchett, J. D. Vervoort, U. Söderlund, *Earth Planet. Sci. Lett.* **222**, 29 (2004).
4. Y. Amelin, W. J. Davis, *Geochim. Cosmochim. Acta* **69**, 465 (2005).
5. G. F. Grinyer *et al.*, *Phys. Rev. C* **67**, 014302 (2003).
6. Y. Nir-El, G. Haquin, *Phys. Rev. C* **68**, 067301 (2003).
7. E. Scherer, C. Münker, K. Mezger, *Science* **293**, 683 (2001).
8. P. J. Patchett, M. Tatsumoto, *Nature* **288**, 571 (1980).
9. J. Blichert-Toft, M. Boyet, P. Telouk, F. Albarède, *Earth Planet. Sci. Lett.* **204**, 167 (2002).
10. M. Bizzarro, J. A. Baker, H. Haack, D. Ulfbeck, M. Rosing, *Nature* **421**, 931 (2003).
11. F. Tera, R. W. Carlson, N. Z. Boctor, *Geochim. Cosmochim. Acta* **61**, 1713 (1997).
12. H. Palme *et al.*, *Geochim. Cosmochim. Acta* **45**, 727 (1981).
13. T. J. McCoy *et al.*, *Geochim. Cosmochim. Acta* **60**, 2681 (1996).
14. M. M. Grady, *Catalogue of Meteorites* (Cambridge Univ. Press, Cambridge, 2000).
15. C. Göpel, G. Manhès, C. J. Allègre, *Meteoritics* **27**, 226 (1992).
16. K. Min, K. A. Farley, P. R. Renne, K. Marti, *Earth Planet. Sci. Lett.* **209**, 323 (2003).
17. G. H. Barfod, E. J. Krogstad, R. Frei, F. Albarède, *Geochim. Cosmochim. Acta* **69**, 1847 (2005).
18. Y. Amelin, A. Ghosh, E. Rotenberg, *Geochim. Cosmochim. Acta* **69**, 505 (2005).
19. Materials and methods are available as supporting material on *Science* Online.
20. According to (*12*), ~90% of Acapulco phosphate is apatite and 10% is merrillite.
21. U-Pb analytical procedure is as described in (*18*), with modifications described in (*22*).
22. A. N. Krot, Y. Amelin, P. Cassen, A. Meibom, *Nature* **436**, 989 (2005).
23. K. R. Ludwig, *Geochim. Cosmochim. Acta* **62**, 665 (1998).
24. A. H. Jaffey, K. F. Flynn, L. E. Glendenin, W. C. Bentley, A. M. Essling, *Phys. Rev. C* **4**, 1889 (1971).
25. K. R. Ludwig, *Chem. Geol.* **166**, 315 (2000).
26. C. Göpel, G. Manhès, C. J. Allègre, *Earth Planet. Sci. Lett.* **121**, 153 (1994).
27. T. R. Ireland, B. Fegley, *Int. Geol. Rev.* **42**, 865 (2000).
28. H. Palme, A. Jones, *Treatise Geochem.* **1**, 41 (2003).
29. F. Albarède *et al.*, *Geochim. Cosmochim. Acta*, in press.

30. I thank K. Marti for the sample of Acapulco, the Mineralogy Department of the Royal Ontario Museum for the sample of Richardton, F. Corfu and M. Bizzarro for aliquots of their Lu-Hf reference solutions, T. Pestaj and J. Peressini for help with mineral separations, and L. Cataldo for help with cleaning the sample introduction system and with maintaining the good working order of the Nu Plasma (Nu Instruments, Wrexham, UK). Comments by D. Davis, B. Davis, F. Albarède, and two journal reviewers improved the paper.

Supporting Online Material

www.sciencemag.org/cgi/content/full/310/5749/839/DC1
Materials and Methods
SOM Text
Fig. S1
Tables S1 to S3
References and Notes

25 July 2005; accepted 4 October 2005
10.1126/science.1117919

The Radiative Signature of Upper Tropospheric Moistening

Brian J. Soden,[1]* Darren L. Jackson,[2] V. Ramaswamy,[3] M. D. Schwarzkopf,[3] Xianglei Huang[4]

Climate models predict that the concentration of water vapor in the upper troposphere could double by the end of the century as a result of increases in greenhouse gases. Such moistening plays a key role in amplifying the rate at which the climate warms in response to anthropogenic activities, but has been difficult to detect because of deficiencies in conventional observing systems. We use satellite measurements to highlight a distinct radiative signature of upper tropospheric moistening over the period 1982 to 2004. The observed moistening is accurately captured by climate model simulations and lends further credence to model projections of future global warming.

The importance of water vapor in regulating climate is undisputed. It is the dominant greenhouse gas, trapping more of Earth's heat than any other gaseous constituent (*1*). As the climate warms in response to increases in other greenhouse gases such as carbon dioxide, the concentrations of water vapor are expected to increase (*2*–*7*). If water vapor concentrations do increase in a warmer world, the added absorption will act to further amplify the initial warming. Models of Earth's climate suggest that this serves as a powerful positive feedback, more than doubling the sensitivity of the surface temperature to an anthropogenic forcing (*8*–*11*).

All climate models predict that the concentration of water vapor in the upper troposphere will increase markedly in the future (*9*, *12*). However, the validity of such projections has been debated for more than a decade (*13*, *14*). Some argue that the concentrations in the upper troposphere might actually decrease in a warmer climate, given the simplified treatment of convection and cloud-related processes in current models and the important role that they play in governing the distribution of moisture (*15*–*17*).

Here, we use climate model simulations and satellite measurements to demonstrate the presence of a distinct radiative signature of upper tropospheric moistening on interannual to decadal time scales. The observed moistening is consistent with model simulations and corresponds approximately to a constant relative humidity increase in upper tropospheric moisture (*18*). We further demonstrate that without such an increase, the model would be unable to reproduce the satellite-observed radiance record.

The distribution of water vapor is highly variable in both space and time. Because the equilibrium vapor pressure of water depends strongly on temperature, the concentration of water vapor diminishes rapidly with height. Yet because the absorptivity of water vapor is proportional to the logarithm of its concentration, it is the fractional change in water vapor mass, not the absolute change, that governs its strength as a feedback mechanism.

Model calculations of the fractional change in global mean water vapor mixing ratio (*19*) using the Geophysical Fluid Dynamics Laboratory (GFDL) atmospheric general circulation model (GCM) (*20*) indicate a distinct upper tropospheric amplification to the simulated changes in water vapor over the past two decades (*21*) (fig. S1). A similar vertical amplification is predicted to occur over the coming century in response to increases in anthropogenic greenhouse gases and is a robust feature of all climate model projections (*9*, *12*, *18*). Simulations of the 21st-century climate from the GFDL coupled ocean-atmosphere model indicate an increase in lower tropospheric water vapor of ~20% by the end of the century, versus an upper tropospheric increase of ~100% (*21*) (fig. S1). Such a difference highlights the importance of upper tropospheric water vapor as a feedback mechanism, and of its measurement as a factor in the detection and attribution of climate change.

Previous studies have demonstrated the presence of regional moistening trends in the lower troposphere since the mid-1970s from radiosonde measurements (*22*, *23*). Increases in the total column water vapor mass (*19*) have

[1]Rosenstiel School for Marine and Atmospheric Science, University of Miami, Miami, FL 33149, USA. [2]Cooperative Institute for Research in Environmental Sciences, University of Colorado, Boulder, CO 80305, USA. [3]Geophysical Fluid Dynamics Laboratory, National Oceanic and Atmospheric Administration, Princeton, NJ 08542, USA. [4]Atmospheric and Oceanic Sciences Program, Princeton University, Princeton, NJ 08542, USA.

*To whom correspondence should be addressed. E-mail: bsoden@rsmas.miami.edu

also been observed over the global oceans since the mid-1980s from satellites (*24*, *25*). These lower tropospheric moistening trends are strongly linked to changes in surface temperature and are consistent with those expected under the assumption of constant relative humidity.

The model used here is an atmospheric GCM integrated with specified sea surface temperatures (SSTs) (*20*). Four sets of model integrations are performed, each starting in January 1982 when satellite-observed SSTs became available, and ending in December 2004. Because the global anomalies of the ensemble members are nearly identical, only the results from the first member are displayed in the figures, but the trends and standard errors of the trends for all members are summarized in Table 1 (*26*).

When forced with observed SSTs, this model successfully reproduces the observed column-integrated moistening changes over this period (Fig. 1). However, because the mass of water vapor decreases rapidly with height, the column integral is primarily weighted by the lower troposphere, and its largely thermodynamic behavior is unsurprising (*21*). Consequently, there is not much debate about the projected increase of column-integrated water vapor in response to global warming, and its agreement with models provides only limited reassurance in their simulation of water vapor feedback (*9*).

In contrast, water vapor in the free troposphere is not so directly constrained by thermodynamic arguments (*21*), and its response to global warming has been the subject of long-standing controversy (*9*, *15*–*17*). Given the radiative importance of moisture changes in the upper troposphere (*9*, *10*), it is important that humidity changes there are demonstrably consistent between models and observations. Although an international network of weather balloons has carried water vapor sensors for more than half a century, changes in instrumentation and poor calibration make such sensors unsuitable for detecting trends in upper tropospheric water vapor (*27*). Similarly, global reanalysis products also suffer from spurious variability and trends related to changes in data quality and data coverage (*24*).

Satellite observations using the High Resolution Infrared Radiometer Sounder (HIRS) provide a global, temporally coherent archive of radiance measurements in the 6.3-μm water vapor absorption band from 1979 to the present. The radiance channel centered at 6.7 μm (channel 12) is sensitive to water vapor integrated over a broad layer of the upper troposphere (200 to 500 hPa) and has been widely used for studies of upper tropospheric water vapor (*28*). Because clouds strongly attenuate the infrared radiation, we restrict our analysis to clear-sky radiances in which the upwelling radiation in channel 12 is not affected by clouds (*29*).

Table 1. The linear least-squares trend (±2 standard errors of the linear trend) for satellite observations and climate model simulations of total column water vapor, T12, T2, and T2 – T12. The standard errors are estimated following Weatherhead *et al*. (*42*). The rightmost column shows the trends for which the GCM-simulated T12 was computed under the "no moistening" scenario (*21*). Satellite observed trends are computed using the SSMI total column water vapor (*25*), HIRS T12 (*21*), and MSU T2 for both RSS (*38*) and UAH (*37*). GCM trends are shown for each of the four model ensemble members. Asterisks denote results shown in Figs. 1 and 2.

Variable	Satellite	GCM	GCM (no moistening)
Total column vapor (%/decade)	1.40 ± 0.78 (SSMI)	1.20 ± 0.98*	
		1.37 ± 0.78	
		1.20 ± 0.78	
		1.32 ± 0.98	
T12 (K/decade)	0.00 ± 0.04 (HIRS)	0.06 ± 0.04*	0.24 ± 0.12*
		0.07 ± 0.04	0.24 ± 0.12
		0.08 ± 0.04	0.26 ± 0.10
		0.06 ± 0.04	0.23 ± 0.12
T2 (K/decade)	0.17 ± 0.08 (RSS)	0.19 ± 0.08*	
	0.08 ± 0.08 (UAH)	0.19 ± 0.08	
		0.21 ± 0.08	
		0.18 ± 0.08	
T2 – T12 (K/decade)	0.17 ± 0.06 (RSS)	0.13 ± 0.08*	–0.04 ± 0.04*
	0.08 ± 0.06 (UAH)	0.12 ± 0.06	–0.05 ± 0.06
		0.14 ± 0.06	–0.05 ± 0.04
		0.13 ± 0.06	-0.05 ± 0.04

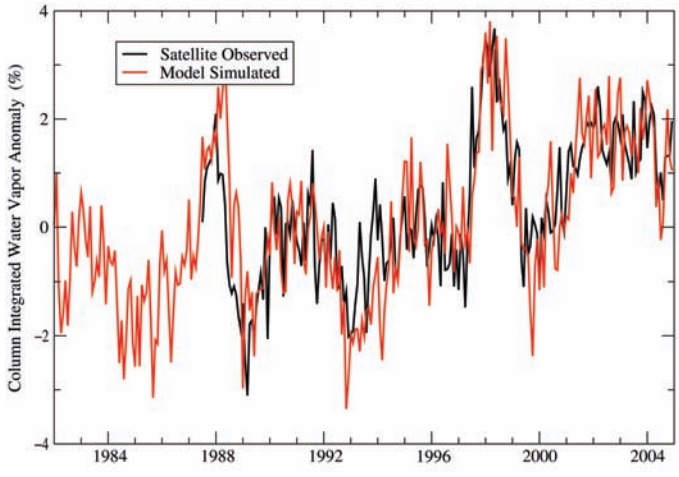

Fig. 1. Global mean (ocean-only) anomalies in column-integrated water vapor from GFDL atmospheric GCM simulations forced with observed SSTs [(*20*); red] and satellite observations from the Special Sensor Microwave Imager (SSMI) [(*25*); black].

Figure 2 compares the satellite-observed equivalent blackbody temperatures from channel 12 (T12) from the HIRS instrument with those computed from the model's temperature and moisture profiles (*30*). Under clear skies, T12 is primarily sensitive to changes in relative humidity averaged over a deep layer of the upper troposphere (roughly 200 to 500 hPa) (*21*). Thus, if the water vapor mass in the upper troposphere increases by conserving relative humidity as the atmosphere warms, only a small perturbation to T12 would be expected.

Although substantial trends in T12 do occur regionally (*31*, *32*), the globally averaged radiance record from HIRS shows little trend over the 20-year period. This lack of trend has been noted in previous studies (*21*, *33*–*36*) and is insensitive to the intercalibration of the radiance records from individual satellites (*21*). The model simulations also yield little trend in global mean T12, implying that there is little change in global mean relative humidity over this period. In fact, the model-simulated anomalies are nearly identical to those obtained if one repeats the calculation of T12 under the assumption of a constant relative humidity change in the model's water vapor field (*21*). This confirms that both the observations and GCM simulations are, to first order, consistent with a constant relative humidity behavior.

In contrast, consider the trend in T12 that would result if there were no increase in water vapor mass in the model's upper troposphere (Fig. 2, top panel, green curve) (*21*). In this case, the T12 would increase by more than 0.5 K over the period from 1982 to 2000, more than four times what was observed, as the result of an increase in Planck emission (warming) without a compensating increase in atmospheric attenuation (moistening). This discrepancy is much larger than the standard error in the trend estimates and is consistent across all GCM ensemble members (Table 1). Thus,

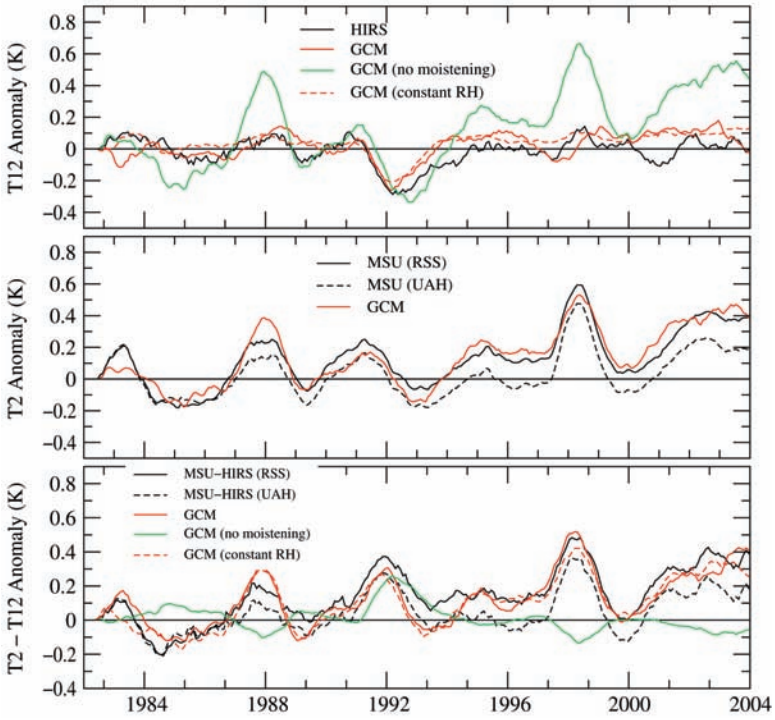

Fig. 2. Global mean time series of T12 (top), T2 (middle), and T2 – T12 (bottom) from GCM simulations (red) and satellite observations (black). The model-simulated radiances are also shown from calculations using a seasonally varying climatological profile with no moistening trend [green line (*21*)] and a prescribed moisture profile that moistens at a constant relative humidity rate [red dashed line (*21*)]. All time series are smoothed with a 6-month running mean.

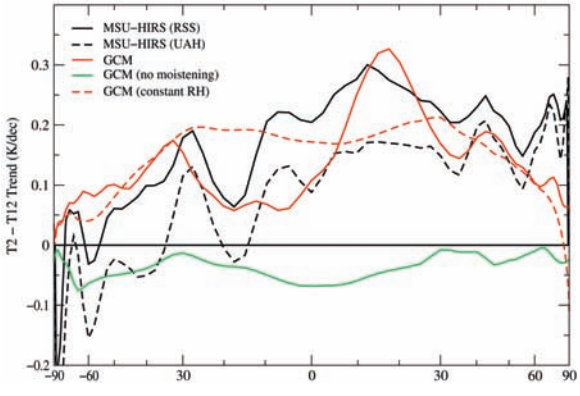

Fig. 3. An area-weighted projection of the zonal mean of the local trend in T2 – T12 (K/decade) for satellite observations (black) and GCM simulations (red). The corresponding trends in T2 – T12 for model-simulated radiances under the constraint of no moistening [green line (*21*)] and constant relative humidity moistening [red dashed line (*21*)] are also shown.

the model would be unable to reproduce the observed radiance record without a nearly constant relative-humidity moistening of the upper troposphere.

Because the anomalies in T12 are a function of both moisture and temperature changes over this period, it is important to verify the credibility of the model-simulated temperature variations. For this purpose, the global mean tropospheric temperature anomalies observed from the Microwave Sounding Unit (MSU) channel 2 radiances (T2) are compared with those simulated from the GCM (Fig. 2, middle panel). The MSU T2 radiances are primarily sensitive to the temperature averaged over a deep layer of the troposphere (roughly 200 to 800 hPa). Observations are shown for both the University of Alabama–Huntsville (UAH) (*37*) and Remote Sensing Systems (RSS) (*38*) versions of MSU channel 2. Over the period 1982 to 2004, the GCM-simulated T2 anomalies are nearly identical in pattern to those observed from MSU, regardless of which record is used. The linear trend of the GCM-simulated T2 (0.18 K/decade) (*21*) is in close agreement with the RSS T2 trend (0.17 K/decade). However, both the GCM and RSS trends are greater than the UAH trend by roughly a factor of 2, reflecting differences between the UAH and RSS reconstruction methods (*38*).

The trends in upper tropospheric water vapor are more easily depicted by differencing the global mean MSU channel 2 and HIRS channel 12 radiance measurements (T2 – T12). As the atmosphere moistens, the emission level for T12 increases as a result of the increasing opacity of water vapor along the satellite line of sight. On the other hand, because the concentration of oxygen does not vary by any appreciable amount, the emission level for the MSU T2 remains constant. Therefore, if the atmosphere moistens, the brightness temperature difference T2 – T12 will increase over time because of the divergence of their emission levels. If, on the other hand, the moisture in the upper troposphere does not increase, the emission level for T12 would remain unchanged, and T2 – T12 would show little change over time.

Both the HIRS observations and GCM simulations indicate an increase in T2 – T12 over this period, reflecting the moistening of the upper troposphere (Fig. 2, lower panel). The model-simulated anomalies in T2 – T12 increase at a rate of 0.14 K/decade from 1982 to 2004. However, if the concentrations of water vapor are held constant when computing the model's T12 (green curve), the trend in T2 – T12 becomes negative (–0.04 K/decade), in stark contrast with that observed.

Both RSS (0.16) and UAH (0.08) reveal increases in T2 – T12 over this period (Fig. 2, lower panel), although the magnitude of the linear trend is roughly twice as large when using RSS T2 than when using UAH T2, reflecting the uncertainty in the rate at which the troposphere has warmed over this period (*38*, *39*). However, it is important to note that although the linear trends differ between the UAH and RSS T2 values, both show similar variability at higher frequencies, and this variability is consistent with a moist-adiabatic warming (*40*) and constant relative humidity moistening of the upper troposphere. In contrast, the "no moistening" version of the model radiance simulations is unable to capture either the observed variability or the linear trend in T2 – T12.

The zonal mean of the trend in T2 – T12 (Fig. 3) further highlights the consistency between the observed and GCM-simulated radiance records, with both showing the largest increases in upper tropospheric water vapor in the tropics and smaller decreases near the poles, including a local maximum in the northern subtropics between 0° and 30°N. In contrast, the zonal mean trends in T2 – T12 for the "no moistening" scenario are negative in most latitudes, in stark contrast to either the HIRS/RSS or HIRS/UAH records. Note that there are regions where the model-simulated trend of T2 – T12 departs substantially from the constant relative humidity approximation, the cause of which warrants further scrutiny.

Upper tropospheric water vapor provides a powerful feedback for amplifying climate change, and its increase is a crucial ingredient to model projections of future global warming. An accurate understanding of the changes in upper tropospheric moisture over time is necessary to verify its role in amplifying climate

sensitivity. Reproduction of the observed radiance record requires a global moistening of the upper troposphere in response to atmospheric warming that is roughly equivalent in magnitude to that predicted under the assumption of constant relative humidity. This behavior is consistent with that simulated from current models and provides key quantitative evidence in support of their ability to predict the climate feedback from upper tropospheric water vapor. Given the importance of water vapor feedback in determining the climatic response to anthropogenic forcings, such confirmation is essential to the use of these models for global warming projections.

References and Notes

1. J. Kiehl, K. Trenberth, *Bull. Am. Meteorol. Soc.* **78**, 197 (1997).
2. U. Cubasch, R. Cess, in *Climate Change: The IPCC Scientific Assessment*, J. T. Houghton *et al.*, Eds. (Cambridge Univ. Press, Cambridge, 1990).
3. R. Cess *et al.*, *J. Geophys. Res.* **95**, 16601 (1990).
4. A. Raval, V. Ramathan, *Nature* **342**, 758 (1989).
5. R. Pierrehumbert, *J. Atmos. Sci.* **52**, 1784 (1995).
6. D. Rind *et al.*, *Nature* **349**, 500 (1991).
7. A. Del Genio, W. Kovari, Y. Mao-Sung, *Geophys. Res. Lett.* **21**, 2701 (1994).
8. T. Stocker *et al.*, in *Climate Change 2001: Contribution of Working Group I to the Third Assessment Report of the Intergovernmental Panel on Climate Change* (Cambridge Univ. Press, Cambridge, 2001), pp. 418–470.
9. I. Held, B. Soden, *Annu. Rev. Energy Environ.* **25**, 441 (2000).
10. R. Colman, *Geophys. Res. Lett.* **31**, L21109 (2004).
11. R. Wetherald, S. Manabe, *J. Atmos. Sci.* **45**, 1397 (1988).
12. B. J. Soden, R. T. Wetherald, G. L. Stenchikov, A. Robock, *Science* **296**, 727 (2002).
13. R. Lindzen, *Bull. Am. Meteorol. Soc.* **71**, 288 (1990).
14. R. E. Dickinson *et al.*, in *Climate Change 1995: The Science of Climate Change*, J. T. Houghton *et al.*, Eds. (Cambridge Univ. Press, Cambridge, 1996), pp. 193–227.
15. D. Sun, R. Lindzen, *J. Atmos. Sci.* **50**, 1643 (1993).
16. R. Lindzen *et al.*, *Bull. Am. Meteorol. Soc.* **82**, 417 (2001).
17. K. Minschwaner, A. Dessler, *J. Clim.* **17**, 1272 (2004).
18. Under a constant relative humidity, the concentration of water vapor is determined by changes in the equilibrium vapor pressure, which increases rapidly with temperature. The Clausius-Clapeyron equation dictates that the fractional increase in equilibrium vapor pressure (e_s) scales according to $d(\ln e_s)/dT \sim 1/T^2$ (where T is absolute temperature). Near the surface, this would lead to roughly a 6% increase in water vapor mass per 1 K warming. In the upper troposphere, where temperatures are colder, the water vapor mass increases at roughly twice this rate (*9*).
19. The water vapor mixing ratio (w) is defined as the mass of water vapor per unit mass of dry air. The relative humidity (r) is determined as the ratio of the water vapor mixing ratio to its "saturated" or equilibrium value (w_s), expressed in percent; $r = 100 \times w/w_s$. The total column water vapor (W) is defined as the vertically integrated mass of water vapor per unit area in units of kg/m^2; $W = \int w\rho\, dz$, where ρ is the density of air and z is altitude, and the integration is performed from the surface to the top of the atmosphere.
20. Model simulations are from the GFDL atmospheric GCM integrated with observed ocean SSTs; see (*41*) for a description of the atmospheric model and SST data set.
21. See supporting data on *Science* Online.
22. R. Ross, W. Elliott, *J. Clim.* **14**, 1602 (2001).
23. P. Zhai, R. Eskridge, *J. Clim.* **10**, 2643 (1997).
24. K. Trenberth, J. Fasullo, L. Smith, *Clim. Dyn.* **24**, 741 (2005).
25. F. Wentz, M. Schabel, *Nature* **403**, 414 (2000).
26. A statistical model (*42*) was used to determine the standard errors of the trends in Table 1. An estimate of the trend (ω) for each time series was determined using a least-squares linear fit. The residual time series, N_t, is defined as the residual time series after removal of the mean, the annual cycle, and the linear trend from the original time series. If we define the variance of N_t as $\sigma^2_N = \mathrm{Var}(N_t)$, then the standard deviation of the trend can be approximated using equation 2 of (*42*) as $\sigma_\omega \approx \sigma_N/n^{3/2}[(1+\phi)/(1-\phi)]^{1/2}$, where the lag-1 autocorrelation is defined as $\phi = \mathrm{Corr}(N_t, N_{t-1})$ and n is the number of years in the monthly mean time series. Table 1 provides $\omega \pm 2\sigma_\omega$ for each time series. A trend may be considered to meet the 95% confidence level when $|\omega| > 2\sigma_\omega$.
27. W. Elliott, D. Gaffen, *Bull. Am. Meteorol. Soc.* **72**, 1507 (1991).
28. B. Soden, F. Bretherton, *J. Geophys. Res.* **98**, 16669 (1993).
29. We use an updated set of clear-sky radiances from HIRS as described in (*32*). Although there could be deficiencies in the cloud-screening methodology that might bias the observed T12, the most recent analysis of cirrus clouds from HIRS, using a method specifically designed to detect thin cirrus, indicates no discernible trend in high-level cloud cover over the period of record (*43*).
30. To avoid uncertainties associated with the inversion of satellite-measured radiances into geophysical quantities, we input the GCM profiles of temperature and water vapor mixing ratio into a narrow-band radiative transfer model to simulate the T12 that the HIRS instrument would have observed under those conditions. The radiative transfer model used here is the HIRS Fast Forward Program (HFFP) (*44*).
31. J. Bates, X. Wu, D. Jackson, *J. Clim.* **9**, 427 (1996).
32. J. Bates, D. Jackson, *Geophys. Res. Lett.* **28**, 1695 (2001).
33. B. Soden, R. Fu, *J. Clim.* **8**, 2333 (1995).
34. A. Geer, J. Harries, H. Brindley, *J. Clim.* **12**, 1940 (1999).
35. R. Allan, M. Ringer, A. Slingo, *Q. J. R. Meteorol. Soc.* **129**, 3371 (2003).
36. M. McCarthy, R. Toumi, *J. Clim.* **17**, 3181 (2004).
37. J. Christy, R. Spencer, W. Braswell, *J. Atmos. Oceanic Technol.* **17**, 1153 (2000).
38. C. Mears, M. Schabel, F. Wentz, *J. Clim.* **16**, 3650 (2003).
39. C. A. Mears, F. J. Wentz, *Science* **309**, 1548 (2005); published online 11 August 2005 (10.1126/science.1114772).
40. B. D. Santer *et al.*, *Science* **309**, 1551 (2005); published online 11 August 2005 (10.1126/science.1114867).
41. Global Atmospheric Model Development Team, *J. Clim.* **17**, 461 (2004).
42. E. C. Weatherhead *et al.*, *J. Geophys. Res.* **103**, 17149 (1998).
43. D. Wylie, D. L. Jackson, W. P. Menzel, J. J. Bates, *J. Clim.* **18**, 3021 (2005).
44. B. Soden *et al.*, *Bull. Am. Meteorol. Soc.* **81**, 797 (2000).

45. Supported in part by the NOAA Office of Global Programs.

Supporting Online Material

www.sciencemag.org/cgi/content/full/1115602/DC1
SOM Text
Fig. S1
References

1 June 2005; accepted 29 September 2005
Published online 6 October 2005;
10.1126/science.1115602
Include this information when citing this paper.

Synthesis of a Stable Compound with Fivefold Bonding Between Two Chromium(I) Centers

Tailuan Nguyen,[1] Andrew D. Sutton,[1] Marcin Brynda,[1] James C. Fettinger,[1] Gary J. Long,[2] Philip P. Power[1]*

Although in principle transition metals can form bonds with six shared electron pairs, only quadruply bonded compounds can be isolated as stable species at room temperature. Here we show that the reduction of $\{Cr(\mu\text{-}Cl)Ar'\}_2$ [where Ar′ indicates C_6H_3-2,6(C_6H_3-2,6-Pr^i_2)$_2$ and Pr^i indicates isopropyl] with a slight excess of potassium graphite has produced a stable compound with fivefold chromium-chromium (Cr–Cr) bonding. The very air- and moisture-sensitive dark red crystals of Ar′CrCrAr′ were isolated with greater than 40% yield. X-ray diffraction revealed a Cr–Cr bond length of 1.8351(4) angstroms (where the number in parentheses indicates the standard deviation) and a planar trans-bent core geometry. These data, the structure's temperature-independent paramagnetism, and computational studies support the sharing of five electron pairs in five bonding molecular orbitals between two $3d^5$ chromium(I) ions.

A quadruple bond between metal centers consisting of σ, 2π, and δ orbital overlaps was shown to be present in salts containing the $[Re_2Cl_8]^{2-}$ ion in 1964 (*1*). Since then, a rich chemistry has developed around this class of transition-metal compounds (*2*), whose bond order exceeds the previously known limit of three for compounds of the p-block elements. Beginning in the mid-1970s, theoretical and spectroscopic investigations of diatomic transition-metal species M_2 (where M is either Cr or Mo) trapped in inert matrices at low temperatures indicated that sextuple bonds consisting of 2σ, 2π, and 2δ overlaps (derived from valence s and d atomic orbitals) could exist between these metals (*3–14*). However, such molecules have no stable existence at room temperature and so cannot be isolated for bulk manipulation.

If ligands are used to stabilize multiply bonded metal centers, their binding reduces the

[1]Department of Chemistry, One Shields Avenue, University of California, Davis, CA 95616, USA. [2]Department of Chemistry, University of Missouri-Rolla, Rolla, MO 65409–0010, USA.

*To whom correspondence should be addressed. E-mail: pppower@ucdavis.edu